# Sound Propagation in hcp Solid Helium Crystals of Known Orientation*

R. H. Crepeau, O. Heybey,† D. M. Lee, and Stanley A. Strauss
*Laboratory of Atomic and Solid State Physics, Cornell University, Ithaca, New York* 14850
(Received 7 August 1970)

Pulse-time-of-flight measurements have been used to determine the velocities of 10-MHz transverse and longitudinal sound in the hcp phase of solid helium-four at a molar volume of approximately 21 $cm^3$ per mole. The measurements have been made on single crystals grown from superfluid helium. The orientations of these crystals have been determined by an optical birefringence technique. The five elastic constants for this molar volume of hcp solid helium have been calculated using the data obtained in these experiments.

## I. INTRODUCTION

Previous measurements on the hcp phase in solid $He^4$ of the longitudinal sound velocity by Vignos and Fairbank[1] and the transverse sound velocity by Lipschultz and Lee[2] have revealed significant anisotropies in these sound velocities. At the time those measurements were made, techniques for determining crystal orientation were not developed, so that a detailed knowledge of sound propagation in solid $He^4$ could not be obtained from the results.

Vos *et al.*[3] and Heybey and Lee[4] have recently shown that optical birefringence measurements could provide a useful method of determining the direction of the $c$ axis in single crystals of hcp solid helium. Measurements of the differences between the ordinary and extraordinary refractive indexes at molar volumes of 21 $cm^3$/mole gave a value of $|n_e - n_0|_{max} = 2.6\times10^{-6}$, corresponding to orthogonality between the $c$ axis and the direction of the light beam, thus showing that centimeter-sized samples of hcp solid $He^4$ corresponded to sizable fractional wavelength shifts between ordinary and extraordinary rays of visible light traversing these samples at appropriate angles.[4]

In this paper, measurements of the transverse and longitudinal sound velocities as a function of crystal direction as determined by these optical methods in hcp solid $He^4$ crystals grown from the superfluid phase of liquid helium are described. From these results, the elastic constants of solid helium are obtained and used to calculate the Debye temperature and the second-sound velocity.

## II. APPARATUS AND EXPERIMENTAL PROCEDURE

### A. Experimental Chamber and Cryogenic Apparatus

A chamber was constructed to allow sound propagation through the solid helium sample in two orthogonal directions and to permit a beam of light to traverse the chamber in a direction perpendicular to the two sound paths. A cross section of the sample chamber assembly is shown in Fig. 1.

This chamber consisted of a copper cube 1.25 in. on a side with $\frac{1}{2}$-in. holes bored through the cube perpendicular to each of the faces. Eight blind bolt holes tapped for 4-40 stainless-steel screws on each face allowed attachment of the window and transducer flanges. Lead gasket seals between the flanges and the chamber proved to be leak tight during the experiment.

The ac-cut 10-MHz quartz sound transducers[5] with gold-plated surfaces were used to generate a transverse (or shear) wave in response to the rf potential applied between the two faces of the transducer. Each of these transducers also produced a longitudinal wave in response to the rf pulse. The horizontal and vertical transducer pairs were mounted such that the axes of each transducer pair (sender and receiver) were parallel in order to ensure a maximum signal. This single transducer orientation was used throughout the experiment and was sufficient to give a wide variety of sound data corresponding to different helium crystal orientations. The transducer flanges were each designed to allow one of the gold-plated surfaces of the transducer to make contact with the smooth surface of the flange. Electrical contact to the front surface of each transducer was made by means of a copper ring insulated from the side of the flange by a thin (0.001-in.) Mylar sheet. The copper ring was held in place with a brass nut and a nylon washer for insulation. A copper-wire lead from the copper ring passed through a short brass capillary soldered into a hole drilled through the transducer flange. A high-pressure seal was made between the copper wire and brass capillary using Stycast[6] 2850 GT Epoxy. This seal was found to be reliable at liquid-helium temperatures after repeated cyclings to room temperature. The copper wire, now outside the pressure chamber, was soldered to a fine coaxial[7] cable which extended to the top of the Dewar and to the outside of the Dewar through a soft solder seal which was vacuum tight. Both ends of the coaxial cable were sealed with Stycast.[6]

The invar support flanges for the Pyrex windows were similar to the transducer flanges except that each window flange had a $\frac{3}{16}$-in. hole drilled through its center for the light beam. The $\frac{1}{8}$-in.-thick Pyrex windows

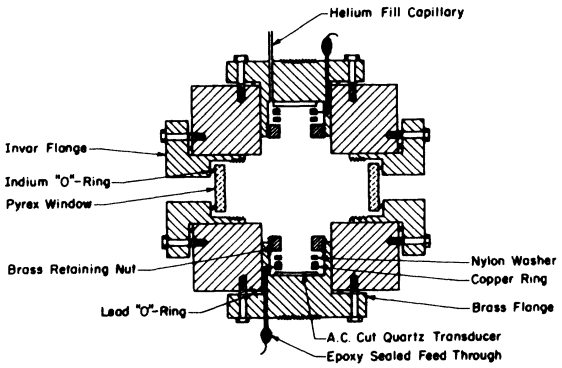


FIG. 1. Cross-sectional view of the sample chamber.

were sealed to the invar with an indium O ring. These flanges were constructed of invar in order to reduce stress birefringence in the Pyrex windows caused by differential expansion during thermal cycling. The procedure for obtaining a satisfactory seal is now described. The 0.015-in. indium wire was wound into about three turns and placed onto the flange, and then the window was pressed into place with a Teflon washer and brass nut. After several hours, the indium made a suitable seal. Then the brass nut and washer were removed, and the flange was ready for mounting. If this seal was found to be leak tight at room temperature, it would generally be superfluid tight at liquid-helium temperatures, although after cycling to room temperature leaks sometimes developed.

The general design of the cryostat is shown in Fig. 2. The sample chamber rested on a copper base that served as a holder for the bottom transducer and as a good conductor of heat. Two copper rods connected this copper flange thermally as well as mechanically to the $He^4$ refrigerator which was in turn suspended in the vacuum space from the bottom flange of the main helium bath container by a stainless-steel pumping tube. By pumping on this helium refrigerator, the temperature of the sample chamber was held near 1.3 °K throughout the data-collecting period. Surrounding the sample chamber and helium refrigerator was a copper shield maintained near liquid-helium temperatures by contact with the main helium bath (at 4.2 °K). Surrounding this shield was an aluminum shield at liquid-nitrogen temperatures. Both the aluminum and copper shields had small holes to allow the laser light beam to pass through the sample chamber and out again. The outer room-temperature Dewar vacuum jacket had two Pyrex windows which were sealed with rubber O rings. This arrangement required only one set of windows at low temperatures and one common vacuum space.

$He^4$ solidifies at a pressure of 25 atm, or greater, and thus a separate system for producing and maintaining this pressure was necessary. The system used in this experiment is shown in Fig. 3. A sample of liquid helium was condensed in a pressure capsule at a temperature of 1.9 °K obtained by pumping on an auxiliary liquid-$He^4$ bath, with helium exchange gas providing the thermal contact between the pumped helium bath and the pressure capsule.

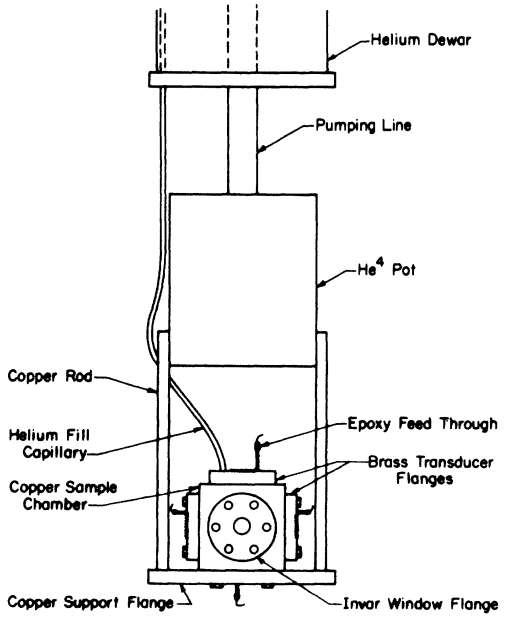


FIG. 2. Schematic drawing of the lower portion of the cryostat.

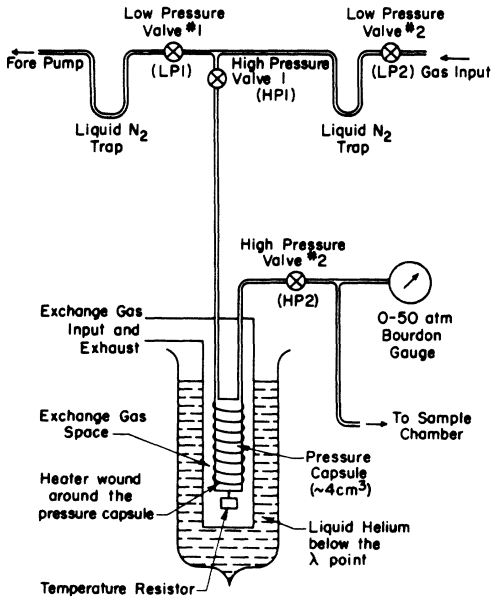


FIG. 3. System used for pressurizing the helium sample.

The exchange gas was then partially removed and an electrical resistance heater was used to raise the temperature of the pressure capsule to 15–20 °K, thus evaporating the helium which had condensed in it. This evaporation gave rise to a large increase in pressure since it occurred in a restricted volume. The pressure was controlled with precision by varying the current through the resistance heater. The pressure capsule was connected to the sample chamber by means of 0.030-in.-o.d. 0.011-in.-i.d. stainless-steel capillary tubing corresponding to the $He^4$ fill capillary shown in Figs. 1 and 2. The pressure capsule near 20 °K also served as a cold trap to purify the helium gas used to form the samples.

### B. Sound-Velocity Measurements and Crystal Growth

The hcp helium crystals examined in this experiment were grown from the superfluid by increasing the pressure at constant temperature. It has been found in these experiments that hcp single crystals could be grown quite readily from the superfluid below 1.45 °K. At higher temperatures the solid grows in the body-centered-cubic phase.[7a]

It was impossible to confirm directly that any given sample grew as a single crystal. It was only after analyzing a great deal of experimental data for a large number of samples that it was possible to infer that most of the samples which gave good transverse and longitudinal sound signals were indeed single crystals.

The procedure used for most of the data contained here is now presented. The pressure was increased to approximately 25.8 atm while a longitudinal sound signal characteristic of the liquid phase was observed on both sets of transducers. At this pressure an hcp solid started to form at the bottom of the sample chamber and a sound signal characteristic of a solid appeared on the horizontal sound path. The vertical sound path continued to show the presence of some liquid in the chamber while the crystal grew to fill the sample chamber. During this growth process, which took two or three minutes, the pressure and temperature of the sample chamber remained constant. The solid-liquid interface and the diffraction pattern produced by the laser shining on this interface were observed during the growth period. It was found experimentally that an uneven surface indicated that crystals of poor quality or polycrystalline samples were being formed, because in these cases transverse sound did not propagate. The completion of the crystal growth was accompanied by the disappearance of the liquid sound signal from the vertical set of transducers.

Once growth of the crystal was complete, the pressure was held constant near the melting curve while the sound-velocity and optical measurements were made. A pulse-time-of-flight method was used to obtain the sound velocities. The output of a pulsed oscillator operating at 10 MHz[8] with pulse width of 2 $\mu$sec and triggered by a time-mark generator[9] was applied to the transmitting quartz transducer. The received signal from the second transducer was amplified by a wide-band amplifier[10] and the output of the amplifier was in turn displayed by one channel of a dual trace-delayed sweep oscilloscope.[11] For the time-of-flight measurement a second output from the time-mark generator was applied directly to the other channel of the oscilloscope. The time-base expander and delay-time adjustment of the oscilloscope made measurement of the leading edge of the initial and received pulse convenient.

The majority of the crystals for which sound pulses were observed were characterized by one transverse and one longitudinal pulse on both the vertical and horizontal sets of transducers as in Fig. 4. On rare occasions, one longitudinal and two transverse signals as shown in Fig. 5 were observed. Usually there were also one or more echoes present on the oscilloscope trace. Attenuation measurements were not performed in this experiment, but typical attenuation lengths in the best crystals were of the same magnitude as those of Lipshultz and Lee.[2]

### C. Optical Measurement and Analysis

When plane-polarized light traverses a uniaxial birefringent medium, such as a crystal of hcp solid helium, it emerges as elliptically polarized light. The characteristics of the resultant elliptically polarized light for various orientations of the initial polarization angle are sufficient to determine the parameters of the birefringent medium, namely, $\delta$, the retardance,[12] and $\beta$, the orientation of the fast axis.[13] Using $\delta$ and $\beta$ for an hcp helium crystal, the angle between the $c$ or optic axis and the direction of light propagation as well as the orientation of the projection of the $c$ axis on a plane perpendicular to

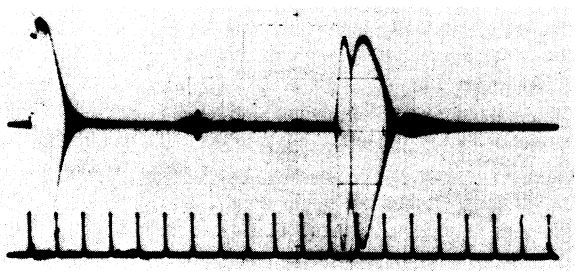

FIG. 4. Photograph of an oscilloscope trace showing a small longitudinal pulse with a time of flight of 55 $\mu$sec and a large transverse pulse with a time of flight of 113 $\mu$sec.

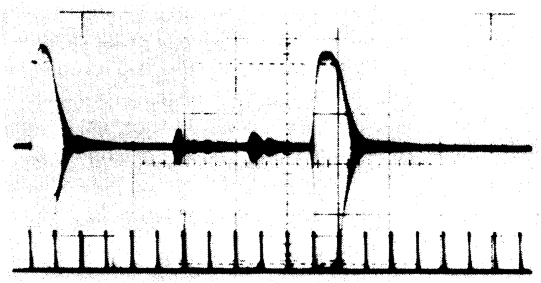

FIG. 5. Photograph of an oscilloscope trace showing a longitudinal pulse at 56 $\mu$sec, a small transverse pulse at 85 $\mu$sec, and a large transverse pulse at 110 $\mu$sec.

the light direction may be found. This information is required in order to determine the direction of the $c$ axis of the crystal relative to the laboratory coordinates and hence relative to the directions of sound propagation.

The ellipse corresponding to the emerging elliptically polarized light is characterized by its ellipticity, the orientation of its major axis relative to some known direction, and its handedness. The ellipticity is the ratio of the minor axis $b$ to the major axis $a$ of the ellipse. In optical measurements an angle $\omega$, defined by $\tan\omega = b/a$, is usually determined. The handedness of the ellipse gives the sense of rotation of the electric vector around the propagation direction of the light. A left-handed ellipse implies that the electric vector rotates counterclockwise when viewed in a direction opposite to that of the light propagation.

In order to determine the characteristics of the emerging elliptically polarized light for each value of the initial plane polarization, the experimental set-up shown in Fig. 6 was used. Unpolarized 6328-Å light from the helium-neon laser was passed through a spinning metal disk with holes uniformly spaced along the circumference of a circle in order to give the light intensity a 600-cycle/sec component. A small portion of the main beam was then reflected for use as a reference to a lock-in amplifier.[14] The remainder of the beam passed through a Nicol prism polarizer to give the beam an initial polarization, and from there passed through the Dewar and sample chamber. A quarter wave plate and a second Nicol prism (the analyzer) were used in series to determine the optical properties of the emerging elliptically polarized light. The detector was a photo-duo-diode[15] connected to the lock-in amplifier. Another photodiode was used to detect the reference signal.

The parameters of the emerging elliptically polarized light were measured for five values of the initial polarization, obtained by rotating the first Nicol prism. For each initial polarization, the quarter wave plate and analyzer were then rotated in a systematic manner until the light intensity reaching the detector was minimized. The positions of the initial polarizer, quarter wave plate, and analyzer were then recorded. The quarter wave plate was then rotated by 90°, without changing the position of the initial polarizer, and the new position of the analyzer for which the transmitted intensity was a minimum was recorded. The minimum in the light intensity at the detector indicated that the elliptically polarized light emerging from the Dewar was converted to linearly polarized light by the quarter wave plate and subsequently blocked by the analyzer. The axes of the quarter wave plate were then parallel to the major and minor axes of the elliptically polarized light. If the fast axis of the quarter wave plate was initially aligned with the major axis of the ellipse, the 90° rotation would result in aligning the fast axis with the minor axis.

The above procedure measures the ellipticity of the elliptically polarized light emerging from the sample chamber, with the help of the relationship $\tan\omega = b/a$, which has been introduced previously. The angle between the orientation of the linearly polarized light emerging from the quarter wave plate and the major axis of the ellipse (and hence one of the axes of the quarter wave plate) is $\omega$. When the quarter wave plate was rotated by 90° the sign of the angle $\omega$ measured from the major axis was changed, but the magnitude of $\omega$ remained the same. Thus the difference in the two recorded positions of the analyzer was equal to $2\omega$.

The procedure is best illustrated by a concrete example. Assume the light emerging from the Dewar is left elliptically polarized with the major axis vertical as shown in the left side of Fig. 7. If the fast axis of the quarter wave plate is aligned with the minor axis, the orientation of the resultant linearly polarized light will be as shown, and $\tan\omega = b/a$. When the quarter wave plate is rotated by 90°, the resultant linearly polarized light will be as in the right side of Fig. 7. The difference

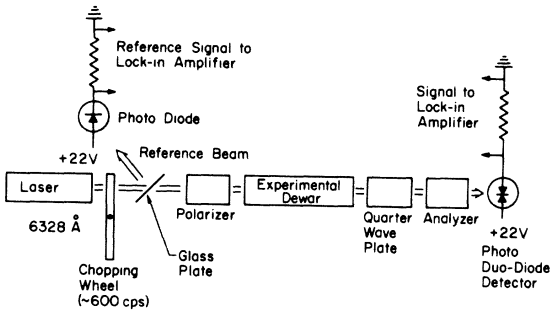


FIG. 6. Block diagram of the optical apparatus.

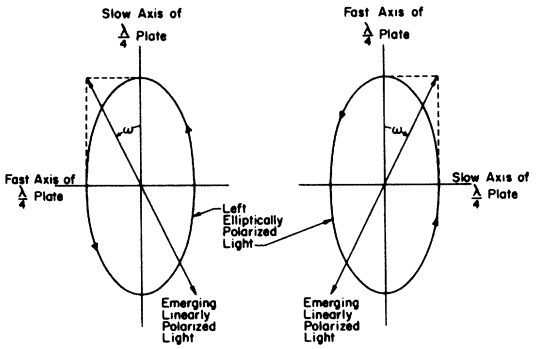


FIG. 7. This figure illustrates how rotating the quarter wave plate through 90° allows measurement of the angle $2\omega$ for left elliptically polarized light.

between the two measured positions of the linearly polarized light is $2\omega$. Note that if the light emerging from the Dewar had been right elliptically polarized, the difference in the two positions would have been $-2\omega$. This procedure eliminates any systematic error in the location of the axis of the quarter wave plate or analyzer.

The maximum value of the phase shift or retardance $\delta$ in these experiments resulting from passage through the sample chamber was about 30°, which leads to a maximum value of 30° for $2\omega$ as will be shown subsequently. Hence the axis of the ellipse which was closest to the orientation of the linearly polarized light emerging from the quarter wave plate was known to be the major axis. Thus always using the same sense of rotation of the quarter wave plate ensured that the sign of the angle $2\omega$ was related to the handedness of the ellipse. The convention used in this experiment for calculating $2\omega$ was to subtract the angle corresponding to the analyzer position when the fast axis of the quarter wave plate was aligned with the major axis of the ellipse from the angular position of the analyzer when the slow axis of the quarter wave plate was aligned with the major axis of the ellipse. These angles were measured in a counterclockwise direction from an arbitrary axis, where the observer was looking into the light source. If Fig. 7 is considered, it becomes evident that a value of $2\omega$ less than zero would imply right elliptically polarized light, while a value of $2\omega$ greater than zero would imply left elliptically polarized light.

When the values of $\sin 2\omega$ were plotted against the orientation of the initial polarization as measured from some arbitrary reference direction, the curve of Fig. 8 represented by Eq. (1) was obtained:

$$\sin 2\omega = \sin\delta \sin 2(\alpha - \beta). \quad (1)$$

In Eq. (1), which is derived in a later section of this paper, $\alpha$ is the orientation of the initial polarization, and $\beta$ is the initial polarization direction for which linearly polarized light emerges from the sample chamber. In order to obtain the values of $\delta$ and $\beta$ from the experimental data, a least-squares fit of the five measured values of $2\omega$ as a function of $\alpha$ was made to Eq. (1). The angle $\delta$ is the retardance of the chamber and its value is seen from Eq. (1) and Fig. 8 to be $\delta = 2\omega_{max}$.

If the sample chamber had been a single birefringent plate, then $\beta$ would have been the orientation of the fast axis of the sample chamber for the case of $2\omega$ changing from (−) to (+) as the initial polarization was rotated counterclockwise. This may be shown by noting that linearly polarized light with an angle of polarization slightly to the right of the fast axis of a birefringent plate produces right elliptically polarized light or $2\omega < 0$. The actual sample chamber consisted of three birefringent plates in series, namely, the entrance and exit windows of the chamber and the helium crystal. Thus $\beta$ was not simply the orientation of the fast axis, although there was a simple relationship between the fast axis of an equivalent birefringent plate and the angle $\beta$ even for this case, as will be shown in the following discussion.

The sample chamber windows were birefringent at low temperatures, probably because of the differential thermal contraction between the windows and the metal flanges. The smallest retardances were observed in Pyrex glass windows with invar flanges, and were on the order of 2°–4° per window. Hence this was the configuration used in the experiment. Quartz windows with invar flanges had a larger birefringence, and quartz or glass windows with brass flanges had phase shifts up to 50° or more at liquid-helium temperatures. Since it was desirable for the phase shift of the helium crystal to be large compared with that of the windows, only those crystals with retardances greater than 10° were judged to provide acceptable data points. The outer room-temperature windows necessary to maintain the vacuum insulation were found to have no significant birefringence.

The method used for determining the window retardances is now described. With the collimated narrow beam of the laser it was possible to observe four reflections from the (very slightly) tilted window, one from the back face of the entrance window, one from the front face of the exit window, and finally one from the back face of the exit window. The retardance for each of these beams was measured without solid in the chamber, giving a set of four values: zero, double the retardance in the entrance window (for two of the reflections), and double the retardance in the combination of both windows. The reflection from the back face of the entrance window was easily identified, since

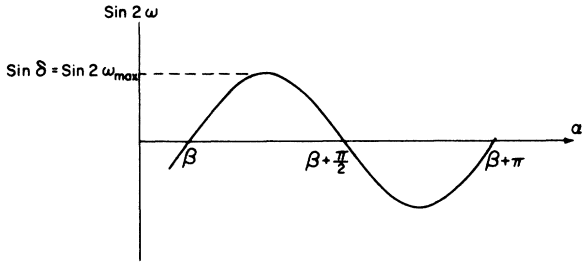


FIG. 8. Plot of $\sin 2\omega$ versus $\alpha$ as given by Eq. (1), $\sin 2\omega = \sin\delta \sin 2(\alpha - \beta)$. $\sin\delta$ is equal to the maximum value of $\sin 2\omega$. The angle $\beta$ is determined from the intersections of curve with the $\alpha$ axis.

the measured retardance was nearly identical to the retardance of the beam reflected from the front face of the exit window. The optical parameters $\delta$ and $\beta$ of the entrance window were then obtained from the measurements and analysis associated with Eq. (1). The corresponding parameters of the exit window were obtained by reversing the direction of the laser beam and repeating the above procedure.

To determine the optical properties of the helium sample from the measured properties of the combination of windows and sample, it was convenient to represent the various optical components by Jones matrices and the polarized light by Jones vectors. The Jones matrix formalism[16] is a compact scheme for writing down the effect of a birefringent plate on the incident polarized light. The notation of Shurcliff[16] is adopted and a complete discussion of Jones matrices can be found in this reference. In this formalism, linearly polarized light is represented as a two-element column matrix of the form

$$\begin{pmatrix}\cos\gamma\\ \sin\gamma\end{pmatrix},$$

where $\gamma$ is positive when it is measured counterclockwise from some arbitrary reference direction with the observer looking into the light source. If the reference direction is taken as the horizontal, the expression

$$\begin{pmatrix}0\\ 1\end{pmatrix}$$

represents vertically polarized light. Elliptically polarized light is represented by a column matrix of the form

$$\begin{pmatrix}A_x \exp(i\epsilon_x)\\ A_y \exp(i\epsilon_y)\end{pmatrix}.$$

Retardation plates are represented in the Jones matrix formalism by a $2\times 2$ matrix which in general has complex elements. The general form for a matrix representing a birefringent plate with retardance $\delta$ and fast axis at some angle $\theta$ with respect to the reference direction is

$$\begin{pmatrix}\cos\frac{1}{2}\delta + i\sin\frac{1}{2}\delta\cos 2\theta & i\sin\frac{1}{2}\delta\sin 2\theta\\ i\sin\frac{1}{2}\delta\sin 2\theta & \cos\frac{1}{2}\delta - i\sin\frac{1}{2}\delta\cos 2\theta\end{pmatrix}.$$

Circular retarders (optically active substances) have the effect of rotating the plane of polarization of linearly polarized light and are represented by a $2\times 2$ matrix having the form of a rotation matrix. If the right circular retardance is $\delta_R$ then the matrix is

$$\begin{pmatrix}\cos\frac{1}{2}\delta_R & \sin\frac{1}{2}\delta_R\\ -\sin\frac{1}{2}\delta_R & \cos\frac{1}{2}\delta_R\end{pmatrix}.$$

Thus the effect of a circular retarder on linearly polarized light is to rotate the direction of the linear polarization by the angle $\frac{1}{2}\delta_R$. The sign of $\delta_R$ is changed for a left circular retarder. Here it is convenient to note that linearly polarized light can be broken up into two counter-rotating circularly polarized components. A difference in refractive index for these two components leads to a net rotation in the plane of polarization when these components are reconstituted into linearly polarized light.

The effect of a series of retarders on incident light is calculated in the Jones matrix formalism by writing down the matrices corresponding to the individual retarders in the same order in which they appear physically and multiplying them out.

The Jones matrix corresponding to a linear retarder will be denoted by the expression $[\delta_i, \theta_i]$ and the Jones matrix corresponding to a circular retarder will be represented by $[\delta_{R_j}]$. Then the matrix corresponding to a combination of linear and circular retarders is given by a product of the form $[\delta_n, \theta_n]\cdots[\delta_{R_m}]\cdots[\delta_1, \theta_1]$ and the column matrix $P_f$ of an emerging beam of polarized light is given in terms of the column matrix $P_0$ of the incident polarized light by the matrix equation

$$P_f = [\delta_n, \theta_n]\cdots[\delta_{R_m}]\cdots[\delta_1, \theta_1]P_0 .$$

As an application of Jones matrices, we shall derive Eq. (1) for a single birefringent plate. If angles are measured from the fast axis of the birefringent plate ($\theta = 0$), linearly polarized light passing through this plate and emerging as elliptically polarized light is described as

$$\begin{pmatrix}\exp(i\delta/2) & 0\\ 0 & \exp(-i\delta/2)\end{pmatrix}\begin{pmatrix}\cos\gamma\\ \sin\gamma\end{pmatrix} = \begin{pmatrix}A_x \exp(i\epsilon_x)\\ A_y \exp(i\epsilon_y)\end{pmatrix}. \quad (2)$$

Recall that Eq. (1) relates the ellipticity $2\omega$ of the emerging elliptically polarized light to the retardance $\delta$ as well as the angle $(\alpha - \beta)$ between the fast axis of the birefringent plate and the polarization vector of the incident linearly polarized light. To obtain this equation, it is convenient to use the following relationship, derived by Born and Wolf,[17] which relates the measured angle $2\omega$ to the parameters of the ellipse on the right-hand side of Eq. (2):

$$\sin 2\omega = -\sin 2(\tan^{-1} A_y/A_x)\sin(\epsilon_y - \epsilon_x) \ .$$

The minus sign appears on the right-hand side of the above equation because our sign convention differs from that of Born and Wolf.

Substituting the expressions $\gamma = \tan^{-1} A_y/A_x$ and $\epsilon_y - \epsilon_x = -\delta$ obtained from solving Eq. (2) into the above equation leads to the following result:

$$\sin 2\omega = \sin 2\gamma \sin\delta \ .$$

With $\alpha$ as the orientation of the initial polarization relative to some arbitrary axis and $\beta$ as the position of the fast axis relative to this arbitrary axis, this equation becomes Eq. (1), i.e.,

$$\sin 2\omega = \sin\delta \sin 2(\alpha - \beta).$$

The optical measurement made on the combination entrance window–crystal–exit window gave the retardance and the orientation of the effective fast axis for the combination. In order to find these parameters for the crystal itself it was necessary to analyze a system of three birefringent plates. This analysis requires use of a theorem[18,19] which shows that any system of $n$ birefringent plates can be replaced by a system of an optical rotator followed by one birefringent plate. In terms of the abbreviations introduced above for the matrices, this theorem is expressed mathematically by the following for the case of three birefringent plates:

$$[\delta_3, \theta_3][\delta_2, \theta_2][\delta_1, \theta_1]\begin{pmatrix}\cos\gamma\\ \sin\gamma\end{pmatrix} = [\delta_e, \theta_e][\delta_R]\begin{pmatrix}\cos\gamma\\ \sin\gamma\end{pmatrix}. \quad (3)$$

Since matrix multiplication is noncommutative, interchanging $[\delta_2, \theta_2]$ with $[\delta_3, \theta_3]$ in the product matrix on the left-hand side of Eq. (3) changes the parameters $\delta_e$, $\theta_e$, and $\delta_R$ on the right. The symbols $\delta_e$ and $\theta_e$ refer to the (hypothetical) equivalent birefringent plate which could be used in conjunction with the rotator $\delta_R$ to produce the same final polarization state as the three plates.

The angle $\delta_e$ is the measured retardance, and $\beta$ is the measured orientation of the initial linear polarization which corresponds to the linearly polarized light entering the sample chamber and emerging as linearly polarized light. The angle $\beta$ is given by $\beta = \theta_e + \delta_R/2$. This equation means that linearly polarized light emerges from the combination of plates when the direction of the initial linearly polarized light is such that the equivalent rotator $[\delta_R]$ rotates the initial linear polarization through an angle of $\delta_R/2$ (clockwise for $\delta_R$ positive) until it is parallel to the fast axis of the equivalent birefringent plate, where the fast axis is designated by the angle $\theta_e$. It is straightforward to demonstrate the validity of Eq. (1) for this more complex case. Equation (3) implies that the matrix product representing the windows and crystal is equal to the product of the matrices representing the equivalent birefringent plate and the optical rotator. If the angles are measured from the fast axis of the entrance window, which is equivalent to setting $\theta_1 = 0$, the matrix equation takes the following form:

$$\begin{bmatrix}\cos\frac{1}{2}\delta_3 + i\sin\frac{1}{2}\delta_3\cos 2\theta_3 & i\sin 2\theta_3\sin\frac{1}{2}\delta_3\\ i\sin 2\theta_3\sin\frac{1}{2}\delta_3 & \cos\frac{1}{2}\delta_3 - i\sin\frac{1}{2}\delta_3\cos 2\theta_3\end{bmatrix}\begin{bmatrix}\cos\frac{1}{2}\delta_2 + i\sin\frac{1}{2}\delta_2\cos 2\theta_2 & i\sin 2\theta_2\sin\frac{1}{2}\delta_2\\ i\sin 2\theta_2\sin\frac{1}{2}\delta_2 & \cos\frac{1}{2}\delta_2 - i\sin\frac{1}{2}\delta_2\cos 2\theta_2\end{bmatrix}$$

$$\times\begin{bmatrix}\cos\frac{1}{2}\delta_1 + i\sin\frac{1}{2}\delta_1 & 0\\ 0 & \cos\frac{1}{2}\delta_1 - i\sin\frac{1}{2}\delta_1\end{bmatrix} = \begin{bmatrix}\cos\frac{1}{2}\delta_e + i\sin\frac{1}{2}\delta_e\cos 2\theta_e & i\sin 2\theta_e\sin\frac{1}{2}\delta_e\\ i\sin 2\theta_e\sin\frac{1}{2}\delta_e & \cos\frac{1}{2}\delta_e - i\sin\frac{1}{2}\delta_e\cos 2\theta_e\end{bmatrix}\begin{bmatrix}\cos\frac{1}{2}\delta_R & \sin\frac{1}{2}\delta_R\\ -\sin\frac{1}{2}\delta_R & \cos\frac{1}{2}\delta_R\end{bmatrix}. \quad (4)$$

The general matrices representing birefringent plates and circular retarders are of the form

$$\begin{bmatrix}A + iB & C + iD\\ -C + iD & A - iB\end{bmatrix}.$$

The product of any number of these matrices will always give a matrix of the same form. Thus Eq. (4) can be reduced to four simultaneous equations, one for each of the terms $A$, $B$, $C$, and $D$. In order to obtain the parameters $\theta_2$ and $\delta_2$ of the helium crystal in terms of the measured quantities $\beta$ and $\delta_e$, we proceed in the following manner, which does not involve an explicit solution of the four simultaneous equations corresponding to Eq. (4). The variables $A$, $B$, $C$, and $D$ of the general matrix form are derived from the right-hand side of Eq. (4) and are thus expressed in terms of $\delta_e$ and $\theta_e$, the param-

eters of the equivalent birefringent plate as well as $\delta_R$, the parameter corresponding to the rotator. This leads to the following expressions:

$$A = \cos\tfrac{1}{2}\delta_e \cos\tfrac{1}{2}\delta_R$$

$$B = \cos 2\theta_e \sin\tfrac{1}{2}\delta_e \cos\tfrac{1}{2}\delta_R - \sin 2\theta_e \sin\tfrac{1}{2}\delta_e \sin\tfrac{1}{2}\delta_R ,$$

$$C = \cos\tfrac{1}{2}\delta_e \sin\tfrac{1}{2}\delta_R ,$$

$$D = \cos 2\theta_e \sin\tfrac{1}{2}\delta_e \sin\tfrac{1}{2}\delta_R + \sin 2\theta_e \sin\tfrac{1}{2}\delta_e \cos\tfrac{1}{2}\delta_R .$$

The following simple relationships are derived from the above equations

$$A^2 + B^2 + C^2 + D^2 = 1, \tag{5}$$

$$\tan\tfrac{1}{2}\delta_R = C/A , \tag{6}$$

$$\tan(2\theta_e + \tfrac{1}{2}\delta_R) = D/B , \tag{7}$$

$$\cos^2\tfrac{1}{2}\delta_e = A^2 + C^2 . \tag{8}$$

If $A$ and $C$ are expressed in terms of the parameters $\theta_1$, $\delta_1$, $\theta_2$, $\delta_2$, $\theta_3$, and $\delta_3$ on the left-hand side of the matrix Eq. (4), the relation (8) $\cos^2\frac{1}{2}\delta_e = A^2 + C^2$ can be used to derive the following, using appropriate trigonometric identities:

$$\begin{aligned}\cos\delta_e &= \cos\delta_2[\cos\delta_1\cos\delta_3 - \sin\delta_1\sin\delta_3\cos 2\theta_2\cos(2\theta_3 - 2\theta_2)] \\ &\quad - \sin\delta_2[\sin\delta_1\cos\delta_3\cos 2\theta_2 + \cos\delta_1\sin\delta_3\cos(2\theta_3 - 2\theta_2)] \\ &\quad + \sin\delta_1\sin\delta_3\sin 2\theta_2\sin(2\theta_3 - 2\theta_2) .\end{aligned} \tag{9}$$

It is now convenient to obtain a relationship between the measured angle $2\beta$ and the parameters in Eq. (4). We recall the fact that $2\beta = 2\theta_e + \delta_R$. Then the tangent of $2\beta$ can be expressed as a function of the tangent of the angle $(2\theta_e + \frac{1}{2}\delta_R)$ and the tangent of the angle $\frac{1}{2}\delta_R$ by using the identity for the tangent of the sum of two angles as follows:

$$\tan 2\beta = \tan(2\theta_e + \delta_R) = \tan[(2\theta_e + \tfrac{1}{2}\delta_R) + \tfrac{1}{2}\delta_R]$$

$$= \frac{\tan(2\theta_e + \frac{1}{2}\delta_R) + \tan\frac{1}{2}\delta_R}{1 - \tan(2\theta_e + \frac{1}{2}\delta_R)\tan\frac{1}{2}\delta_R} .$$

The terms on the right-hand side of this equation can be expressed in terms of $A$, $B$, $C$, and $D$ by substitution using Eqs. (6) and (7) to obtain

$$\tan 2\beta = \frac{D/B + C/A}{1 - DC/AB} = \frac{AD + BC}{AB - DC} .$$

The variables $A$, $B$, $C$, and $D$ are expressed in terms of the parameters $\delta_1$, $\delta_2$, $\delta_3$, $\theta_2$, and $\theta_3$ leading, after lengthy algebra, to the following:

$$\begin{aligned}&\sin\delta_3[\cos 2\theta_2 \sin(2\theta_3 - 2\theta_2) + \sin 2\theta_2\cos(2\theta_3 - 2\theta_2)\cos\delta_2] + \cos\delta_3\sin 2\theta_2\sin\delta_2 \\ &\quad + \{\cos\delta_1\sin\delta_3\sin 2\theta_2\sin(2\theta_3 - 2\theta_2) - [\sin\delta_1\cos\delta_3 + \cos\delta_1\sin\delta_3\cos 2\theta_2\cos(2\theta_3 - 2\theta_2)]\cos\delta_2 \\ &\quad + [\sin\delta_1\sin\delta_3\cos(2\theta_3 - 2\theta_2) - \cos\delta_1\cos\delta_3\cos 2\theta_2]\sin\delta_2\}\tan 2\beta = 0.\end{aligned} \tag{10}$$

Equations (9) and (10) were then solved simultaneously on the Cornell IBM 360/65 computer to give the parameters characterizing the crystal itself, that is, $\theta_2$ and $\delta_2$ .

The orientation of the sound propagation directions relative to the $c$ axis of a given crystal were obtained from the optical measurements of $\delta_2$ and $\theta_2$ for that crystal in the manner described below. The optical retardance $\delta$ represents a phase shift between the plane-polarized ordinary and extraordinary rays, which have orthogonal $\vec{E}$ vectors. The retardance $\delta$ for a uniaxial crystal varies from a maximum for light propagation perpendicular to the optic axis to zero for light propagation along the optic axis. The value of $\delta$ for an arbitrary direction of light propagation is given in terms of the difference between the ordinary and extraordinary refractive indexes $(n_e - n_0)$ for this propagation direction and path length by the equation

$$\delta = (2\pi/\lambda)(n_e - n_0)\, d .$$

The angle $\psi$ between the $c$ axis of the crystal and the light path (see Fig. 9) was calculated from Eq. (11). This equation was derived[20] from the velocity surfaces of a uniaxial crystal and the condition $|n_e - n_0|_{\max} \ll 1$:

$$\sin^2\psi = \frac{[n_e - n_0]}{[n_e - n_0]_{\max}} = \frac{\delta}{\delta_{\max}} . \tag{11}$$

The maximum retardance $\delta_{\max}$ was calculated from the known value of $|n_e - n_0|_{\max}$ for hcp solid $He^4$ and from the known length of the optical path through the chamber.

Since Vos *et al.*[3] have shown that $(n_e - n_0)_{\max} > 0$, the $c$ axis of an hcp helium crystal coincides with

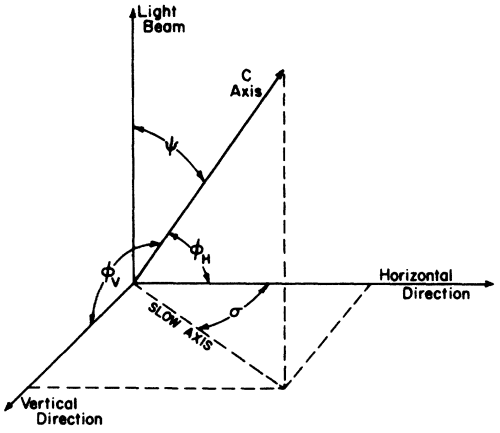


FIG. 9. This figure shows how the $c$-axis orientation is related to the axes of the chamber corresponding to the sound propagation directions.

the slow axis for the special case of light propagation perpendicular to the $c$ axis. It can also be shown in general that for light propagation in an arbitrary direction, the slow (optic) axis of the helium crystal coincides with the projection of the $c$ axis on a plane perpendicular to the light propagation direction.[21] Thus from the calculated value of $\theta_2$, the orientation of the fast axis of the helium crystal relative to the known orientation of the fast axis of the first window, we find the angle $\sigma$, which measures the orientation of the projection of the $c$ axis on the plane perpendicular to the light beam relative to the horizontal.

Using these values of $\psi$ and $\sigma$, the angles $\varphi_H$ and $\varphi_V$ between the $c$ axis of the crystal and the directions of the horizontal and vertical sound paths were calculated from the equations

$$\cos\varphi_H = \sin\psi\cos\sigma\,, \qquad \cos\varphi_V = \sin\psi\sin\sigma\,, \tag{12}$$

which were obtained in a straightforward manner from Fig. 9.

## III. RESULTS AND DISCUSSION

The sound velocities for hcp $He^4$ were measured at pressures close to the melting pressure at 1.32 °K corresponding to a molar volume of 20.97 $cm^3$/mole.[21a] The longitudinal- and the two transverse-mode sound velocities as a function of the angle $\varphi$ between the sound propagation direction and the $c$ axis of the crystal are shown on a polar plot in Fig. 10. The hcp crystal symmetry implies that the sound velocities depend only on the angle between the $c$ axis of the crystal and the direction of the sound path, and not on the azimuthal angle around the $c$ axis. This result is obtained by Zener[22] for a Hooke's law solid with hexagonal symmetry and is also discussed by Musgrave[23] and Gillis *et al.*[24] We follow the latter authors in applying this result to solid helium. The limited amount of scatter in the data of Fig. 10 experimentally justifies the assumption that the sound velocities depend solely on $\varphi$.

These results clearly show the anisotropy indicated in the earlier sound velocity results of Vignos and Fairbank[1] and Lipschultz and Lee[2]. The data are in fair agreement with the phonon spectrum, extrapolated to low $k$ vectors, obtained by slow-neutron scattering from hcp solid $He^4$ at a molar volume of 21.1 $cm^3$/mole at Brookhaven National Laboratory.[25]

The velocities are plotted as a function of $\sin^2\varphi$ in Fig. 11. The curve corresponding to the longitudinal mode has a shape which is very similar to a corresponding curve obtained by Wanner and Franck[26] at considerably higher densities. These investigators also used optical birefringence to obtain the orientations of their $He^4$ crystals. The angular dependence of the sound velocities obtained in our measurements agrees qualitatively with the theoretical predictions of Gillis, Koehler, and Werthamer.[24]

A knowledge of the magnitude and the angular dependence of the sound velocities of solid helium

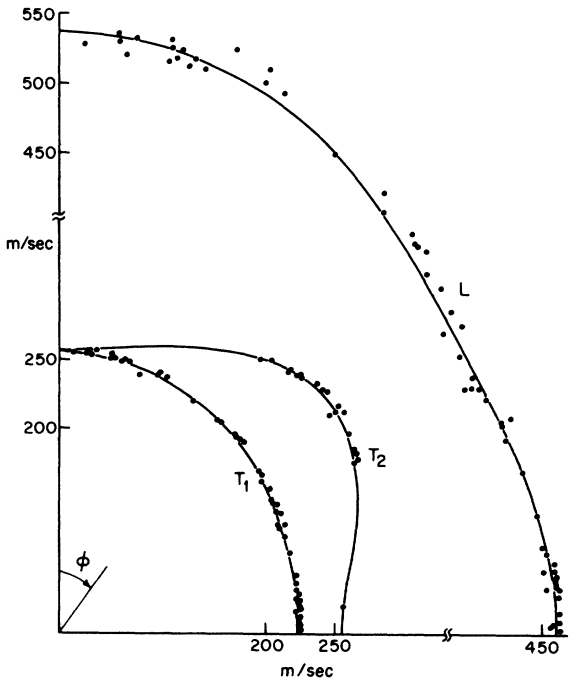


FIG. 10. Polar plot of the various sound velocities as a function of angle $\varphi$, the angle between the sound propagation direction and the $c$ axis of the helium crystal.

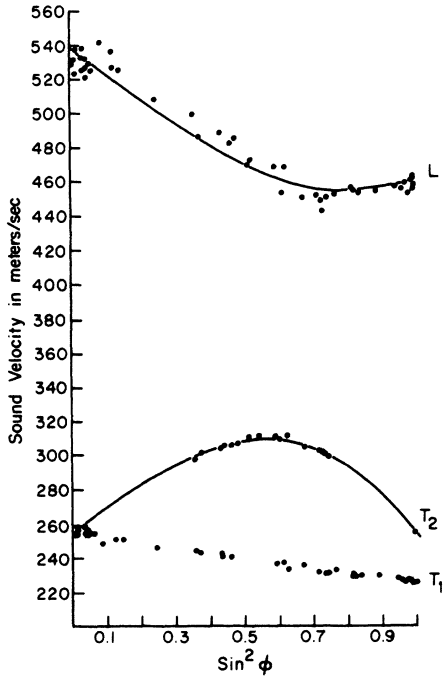


FIG. 11. Plot of the sound velocities versus $\sin^2\varphi$ for hcp solid $He^4$ at molar volume 20.97 $cm^3$/mole.

permits a calculation of the elastic constants. Musgrave[23] has written a comprehensive review of methods of calculating sound velocities in terms of the elastic constants in crystals of various symmetries obeying Hooke's law, and his notation and procedures are used extensively in the discussion of these results. We assume these methods are applicable to solid helium. The form of the velocity surfaces in crystals of hexagonal symmetry may be described in terms of five independent elastic constants: $c_{11}$, $c_{12}$, $c_{13}$, $c_{33}$, and $c_{44}$. Using Musgrave's notation, with $\rho$ equal to the helium density and

$$a = c_{11} - c_{44}, \qquad h = c_{33} - c_{44},$$

$$c = c_{11} - c_{12} - 2c_{44}, \quad H = \rho v^2 - c_{44},$$

$$d = c_{13} + c_{44},$$

the determinantal cubic equation for the velocity surface becomes

$$H^3 - [n^2 h + (1-n^2)(a + \tfrac{1}{2}c)]H^2 + (1-n^2)\{(1-n^2)\tfrac{1}{2}ac + n^2[h(a+\tfrac{1}{2}c) - d^2]\}H - \tfrac{1}{2}n^2(1-n^2)^2 c(ah - d^2) = 0, \qquad (13)$$

where the $(l, m, n)$ correspond to direction cosines of the phase velocity relative to the $x$, $y$, and $z$ axes, respectively, where $z$ is the direction of the $c$ axis of the crystal and $x$ and $y$ are in the basal plane. The absence of $l$ and $m$ in this equation indicates that the velocities depend only on the angle between the direction of propagation and the $z$ axis, and that the velocity surfaces possess circular symmetry about the $z$ axis. The three solutions to this cubic equation are labeled $H_L$, $H_{T_1}$, and $H_{T_2}$ corresponding to the quasilongitudinal, pure-transverse, and quasitransverse modes, respectively.

For a quick determination of some of the elastic constants, it may be noticed that in the basal plane with $n = 0$

$$H_L = a, \qquad H_{T_1} = \tfrac{1}{2}c, \qquad H_{T_2} = 0,$$

or

$$\rho v_L^2 = c_{11}, \quad \rho v_{T_1}^2 = \tfrac{1}{2}(c_{11} - c_{12}), \quad \rho v_{T_2}^2 = c_{44}$$

and along the $z$ or $c$ axis, $n = 1$ and

$$H_{T_1} = 0, \qquad H_L = h, \qquad H_{T_2} = 0,$$

or

$$\rho v_{T_1}^2 = c_{44}, \quad \rho v_L^2 = c_{33}, \quad \rho v_{T_2}^2 = c_{44}.$$

Thus the velocities along the $c$ axis and in the basal plane allow determination of $c_{11}$, $c_{12}$, $c_{33}$, and $c_{44}$. The constant $c_{13}$ may then be found by taking the data at some intermediate angle and solving the cubic equation for $c_{13}$.

In obtaining the elastic constants from the results, we have used a method which made use of all of the data in a somewhat more systematic way. The cubic [Eq. (13)] has three solutions for $H$ and consequently three solutions for $v^2$. One solution yields the values for the velocity of a purely transverse mode $T_1$. The other two solutions consist of mixtures of transverse and longitudinal modes. One of the solutions is preponderantly longitudinal and consequently is called a quasilongitudinal mode, labeled $L$. The other solution is preponderantly transverse and hence is called a quasitransverse mode, labeled $T_2$.

The cubic can be factored into a linear term for $T_1$ and a quadratic term for $T_2$ and $L$, leading to the following equations:

$$H_{T_1} - \tfrac{1}{2}m^2 c = 0, \qquad (14)$$

$$H_{T_2,L}^2 - (m^2 a + n^2 h) H_{T_2,L} + m^2 n^2 (ah - d^2) = 0. \qquad (15)$$

Because of the circular symmetry around the $z$ axis, we set $l = 0$ so that $1 - n^2$ in Eq. (13) is replaced by $m^2$.

Using the known velocities for the various crystal orientations and the above equations, the reduced elastic constants, that is, the elastic con-

stants divided by the density, were calculated. The least-square technique used was to first fit the $T_1$ data to Eq. (14) and solve for $c$ and $c_{44}$. Then, using these values of $c_{44}$ and $c$, the $T_2$ and $L$ data were fitted to Eq. (15), and the remaining fit parameters $a$, $h$, and $(ah-d^2)$ were obtained. An initial estimate of the reduced elastic constants was found by using an unweighted least-squares fit. Then a better fit was obtained by employing a technique recently developed by Gerhold.[27] This technique minimizes a weighted sum of the square of the perpendicular distances from the data points to the parametrized curve. The fit was programmed on the Cornell IBM 360/65 computer and the results are shown in Table I. The solid curves drawn in Figs. 10 and 11 are calculated from the values of the elastic constants obtained from the fit parameters of the least-squares fit.

In the last column of Table I, the estimated maximum uncertainty from all sources is listed. This includes the random error calculated from the scatter of the data and possible systematic errors in the values of $|n_e-n_0|_{max}$, the measured lengths of the sound paths, the optical measurements, and the values of window retardance. It should be noted that $c_{13}$ has a larger uncertainty than the other elastic constants. The reason for this larger uncertainty becomes apparent from a consideration of the magnitude of $c_{13}$ relative to the other elastic constants and the method of calculating $c_{13}$ from the fit parameters. The third column of Table I gives an estimate of the uncertainty in the values of the elastic constants resulting exclusively from the uncertainty quoted by Heybey and Lee[4] for $|n_e-n_0|_{max}$ of $\pm 4\%$ for 6328-Å light passing through a crystal of hcp $He^4$ with molar volume 20.97 $cm^3$/mole. The uncertainty in the elastic constants comes about as a result of the uncertainty introduced into the angular dependence of the sound velocities produced by this uncertainty in $|n_e-n_0|_{max}$. Since, according to Eqs. (11) and (12), $\cos\varphi_H$ and $\cos\varphi_V$ are proportional to $[(n_e-n_0)/(n_e-n_0)_{max}]^{1/2}$, a 4% uncertainty in $(n_e-n_0)_{max}$ would lead to 2% uncertainty in $\cos\varphi_H$ and $\cos\varphi_V$. This uncertainty is used to estimate the systematic error in the elastic constants with the help of Eqs. (14) and (15). It should be noted in Fig. 11 that the scatter in the longitudinal sound data is considerably larger than that for the transverse data. Since the transducers used in the experiment were shear transducers, the longitudinal sound signals were rather weak, resulting in greater difficulty in determining the arrival time of the longitudinal sound pulses as compared with that of the transverse pulses.

TABLE I. Elastic constants of hcp solid helium-four, molar volume 20.97 $cm^3$/mole.

| Reduced elastic constant | Value ($cm^2/sec^2$) | Systematic uncertainty from $\pm 4\%$ in $n_e-n_0$ | Total uncertainty |
|---|---|---|---|
| $c_{11}$ | $2.12\times10^9$ | $\mp 0.28\%$ | $\pm 1\%$ |
| $c_{33}$ | $2.90\times10^9$ | $\pm 2.0\%$ | $\pm 4\%$ |
| $c_{44}$ | $6.52\times10^8$ | $\pm 0.9\%$ | $\pm 2\%$ |
| $c_{12}$ | $1.11\times10^9$ | $\mp 0.59\%$ | $\pm 2\%$ |
| $c_{13}$ | $5.49\times10^8$ | $\pm 3.1\%$ | $\pm 12\%$ |

TABLE II. Comparison of values of the Debye temperature of hcp solid $He^4$.

| Measurement | $\theta$(°K) | $V$($cm^3$/mole) | $T$(°K) |
|---|---|---|---|
| Calculated from these results by Strauss (Ref. 28) | 26.0 | 20.97 | 1.32 |
| Calculated from these results by Wanner and Franck (Ref. 29) | 25.87 | 20.97 | 1.32 |
| Edwards and Pandorf (Ref. 31) | 24.3 | 20.93 | 1.25 |
| Edwards and Pandorf (Ref. 31) extrapolated to $T=0$ | 26.35 | 20.93 | 0 |
| Ahlers (Ref. 33) | 23.4 | 20.9 | $\simeq 1.45$ |
| Heltemes and Swenson (Ref. 32) | $24.6\pm0.6$ | 21.04 | 1.45 |

The knowledge of the elastic constants obtained in this experiment allows a calculation of the Debye temperature. Calculations have been performed by Strauss[28] and by Wanner and Franck[29] using our experimental data. The former author, using the method of Fedorov,[30] obtained a Debye temperature for hcp solid $He^4$ at a molar volume of 20.97 $cm^3$/mole of 26.0 °K. The latter authors obtained a value of 25.87 °K by direct numerical integration. These values of the Debye temperature are to be compared with the Debye temperature obtained from the specific-heat measurements performed by Edwards and Pandorf,[31] Heltemes and Swenson,[32] and Ahlers[33] on solid $He^4$ with molar volume appropriate to our experiment. Comparisons between the various values of Debye temperature are given in Table II.

The agreement between the Debye temperature calculated from these results and the specific-heat data is good, especially since the optical modes do not contribute to the Debye temperatures obtained from our acoustic data. At absolute zero, the optical modes are unpopulated and hence they do not contribute to the specific heat. The Debye temperature of Edwards and Pandorf extrapolated to absolute zero gives a value of 26.35 °K. The agreement between this value of the Debye temperature and the values obtained from the present work is

indeed excellent.

Strauss[28] has also calculated the velocity of second sound from our elastic constants to be 156 m/sec in the isotropic approximation, again using the method of Fedorov. This result is to be compared with the experimental value 125 m/sec obtained from the work of Ackerman and Guyer[34] by extrapolating their data to a molar volume of 21 $cm^3$/mole.

## IV. CONCLUSION

In this work, measurements have been reported of a complete set of sound velocities, longitudinal and transverse, for a large number of crystal orientations, allowing calculation of the elastic constants of hcp solid $He^4$ for the molar volume 20.97 $cm^3$/mole. The method of determining the orientation of the $c$ axis of the hexagonal crystals by means of optical birefringence was successfully applied. A large number of samples were investigated due to the relative ease of growing large helium crystals from the superfluid phase of liquid helium. Extending these measurements to higher densities would be more difficult, since this would require crystal growth from the nonsuperfluid phase of liquid helium. Although such a technique is highly developed,[35] the time required to grow a crystal is quite long, and since a large quantity of data must be collected to obtain elastic constants, a great deal of time would have to be devoted to conduct a comparable investigation at higher densities. Such an investigation is now in progress at the University of Alberta.[26] The optical birefringence method should be applicable to investigation of other orientation-dependent properties of solid helium such as thermal conductivity measurements where interesting anisotropies have recently been observed.[36,37] Competitive methods of determining crystal orientation are neutron diffraction[25] and x-ray diffraction.[38,39] The neutron diffraction method is not applicable to $He^3$ because of the large inelastic neutron scattering cross section. The optical birefringence method cannot be applied to the bcc phase since crystal symmetry precludes the possibility of double refraction in this phase of solid helium. The x-ray method is applicable to all isotopes and phases of solid helium, and hence is the most general method for obtaining crystal orientation. Measurements of sound velocity as a function of crystal direction have recently been reported for bcc solid $He^3$ as well as hcp solid $He^4$ in which the crystal orientations were obtained using x-ray diffraction.[40,41]

## ACKNOWLEDGMENTS

It is a pleasure to thank Dr. N. R. Werthamer, Professor L. Nosanow, Professor R. A. Guyer, Professor G. V. Chester, and Professor J. A. Krumhansl for many valuable discussions concerning solid helium. We are also grateful to Professor Paul L. Hartman, Professor John D. Reppy, and Professor F. P. Lipschultz for important suggestions regarding experimental technique. Finally, we are indebted to Dr. R. Wanner and Professor J. P. Franck, who have been conducting a parallel investigation at the University of Alberta, for informing us of their results and progress throughout the course of these measurements.

---

*Work supported by the National Science Foundation (GP-8148) and by the Advanced Research Projects Agency through the Materials Science Center at Cornell University.

†Present address: Department of Physics, Rice University, Houston, Tex.

[1]J. H. Vignos and H. A. Fairbank, Phys. Rev. 147, 185 (1966).

[2]F. P. Lipschultz and D. M. Lee, Phys. Rev. Letters 14, 1017 (1965).

[3]J. E. Vos, R. V. Kingma, F. J. Van der Gaag, and B. S. Blaisse, Phys. Letters 24A, 738 (1967); J. E. Vos, B. S. Blaisse, D. A. E. Boon, W. J. Van Scherpenzeel, and R. Kingma, Physica 37, 51 (1968).

[4]O. W. Heybey and D. M. Lee, Phys. Rev. Letters 19, 106 (1967).

[5]Valpey Corporation, Holliston, Mass. and Newport Beach, Calif.

[6]Emerson and Cuming, Inc., Canton, Mass.

[7]Uniform Tubes, Inc., Collegeville, Penn.

[7a]A. F. Schuch and R. L. Mills, Phys. Rev. Letters 8, 469 (1962).

[8]Arenberg Ultrasonic Laboratory, Inc., Jamaica Plain, Mass., Model PG-650C pulsed oscillator.

[9]Tektronix, Inc., Beaverton, Ore. Type RM 181 Time-Mark Generator.

[10]Arenberg Ultrasonic Laboratory, Inc., Jamaica Plain, Mass., Model WA-600-C wide-band amplifier.

[11]Tektronix, Inc., Beaverton, Ore., Type 547 Oscilloscope with type CA dual trace plug-in unit.

[12]The retardance $\delta$ of a birefringent medium is defined as the optical phase shift between the ordinary and extraordinary rays. A complete discussion is given by William A. Shurcliff, *Polarized Light* (Harvard U. P., Cambridge, Mass., 1962), p. 89.

[13]The fast axis of a uniaxial birefringent medium for a given light path is the direction of the $E$ vector of the incident light which corresponds to maximum speed of propagation through the medium. See Shurcliff (Ref. 12, p. 69) for a more complete definition of the fast and slow axes.

[14]Princeton Applied Research Corporation, Princeton, N. J.

[15]Texas Instruments, Inc., Houston, Tex., Type 1N2175.

[16]William A. Shurcliff, Ref. 12, Chap. 8.

[17]M. Born and E. Wolf, *Principles of Optics* (Pergamon, New York, 1959), p. 26.

[18]H. Poincaré, *Théorie Mathématique de la Lumière* (G. Carre, Paris, 1892), Vol. II, Chap. XII.
[19]H. Hurwitz and R. Clark Jones, J. Opt. Soc. Am. 31, 493 (1941).
[20]M. Born and E. Wolf, Ref. 17, p. 696.
[21]M. Born and E. Wolf, Ref. 17, p. 677.
[21a]E. R. Grilly and R. L. Mills, Ann. Phys. (N.Y.) 18, 250 (1962).
[22]Clarence Zener, Phys. Rev. 49, 122 (1935).
[23]M. J. P. Musgrave, in *Reports on Progress in Physics*, edited by A. C. Stickland (The Physical Society, London, 1959), Vol. XXII, p. 74.
[24]N. S. Gillis, T. R. Koehler, and N. R. Werthamer, Phys. Rev. 175, 1110 (1968).
[25]V. J. Minkiewicz, T. A. Kitchens, F. P. Lipschultz, R. Nathans, and G. Shirane, Phys. Rev. 174, 267 (1968); F. P. Lipschultz, V. J. Minkiewicz, T. A. Kitchens, G. Shirane, and R. Nathans, Phys. Rev. Letters 19, 1307 (1967).
[26]R. Wanner and J. P. Franck, Phys. Rev. Letters 24, 365 (1970).
[27]S. A. Gerhold, Am. J. Phys. 37, 156 (1969).
[28]Stanley A. Strauss, Solid State Commun. 8, 1325 (1970).
[29]R. Wanner and J. P. Franck (private communication).
[30]F. I. Fedorov, *Theory of Elastic Waves in Crystals* (Plenum, New York, 1968), p. 339.
[31]D. O. Edwards and R. C. Pandorf, Phys. Rev. 140, A816 (1965).
[32]E. C. Heltemes and C. A. Swenson, Phys. Rev. 128, 1512 (1962).
[33]G. Ahlers, Phys. Rev. 135, A10 (1964).
[34]C. C. Ackerman and R. A. Guyer, Ann. Phys. (N.Y.) 50, 128 (1968).
[35]L. P. Mezhov-Deglin, Zh. Eksperim. i Teor. Fiz., 49, 66 (1965) [Soviet Phys. JETP 22, 47 (1966)].
[36]B. Bertman, H. A. Fairbank, R. A. Guyer, and C. W. White, Phys. Rev. 142, 79 (1966).
[37]E. M. Hogan, R. A. Guyer, and H. A. Fairbank, Phys. Rev. 185, 356 (1969).
[38]Samuel C. Fain, Jr., thesis University of Illinois, Urbana, Ill., 1969 (unpublished).
[39]R. L. Mills and A. F. Schuch, in *Proceedings of the Eighth International Conference on Low Temperature Physics* (Butterworths, Washington, 1963), p. 423.
[40]D. S. Greywall and J. A. Munarin, Phys. Rev. Letters 24, 1282 (1970).
[41]D. S. Greywall and J. A. Munarin, Bull. Am. Phys. Soc. 15, 531 (1970).

PHYSICAL REVIEW A VOLUME 3, NUMBER 3 MARCH 1971

# Transport Theory for a Two-Dimensional Dense Gas

Y. Pomeau
*Laboratoire de Physique des Plasmas, Faculté des Sciences-91-Orsay, France*
(Received 6 August 1969; revised manuscript received 8 September 1970)

A kinetic theory has been proposed by several authors with the goal of eliminating the divergences which appear in the density expansion in nonequilibrium systems. Here, it is shown that for a two-dimensional simple gas the theory presents a new divergence, resulting from the fact that correlations propagate over long distances as a result of hydrodynamic transport. This divergence is discussed explicitly for a gas model: the Maxwell model. It will be indicated why the kinetic theory for a perfect Lorentz gas does not exhibit this new divergence.

## I. INTRODUCTION

Near the perfect-gas state, equilibrium quantities of a classical fluid can be calculated by means of the virial expansion. In the same manner, nonequilibrium quantities such as viscosity or thermal conductivity can be expanded in powers of density. One can also develop the collision operator of the kinetic theory in powers of the density $n$. In the lowest order in $n$, one finds the Boltzmann kinetic equation, then the Choh-Uhlenbeck equation, [1] etc. This second approximation in $n$ implies an explicit solution of the three-body problem, so that any calculation to this order would be difficult. However, it has been shown[2] that the shear viscosity of a gas of hard disks, at the Choh-Uhlenbeck order, leads to a diverging integral, and that presumably the same difficulty arises with the next higher order of density for a gas of hard spheres.

A theory has been proposed[3] with the goal of eliminating these divergencies: The transport coefficients are developed in powers of the density. Summing in each order the most divergent contributions, one is led to a renormalized Choh-Uhlenbeck collision operator, called the "ring-collision operator." This operator brings into effect the collective dynamics for calculation of the long-range correlation. In Sec. II we derive this ring-collision operator in a manner slightly different from those given previously. [3]

The Green's function for the linearized Boltzmann equation appears in the ring-collision operator. In the general case, one cannot find this Green's function explicitly. Nevertheless one knows its properties for those disturbances which propagate at long range, i.e., in the hydrodynamical limit. The

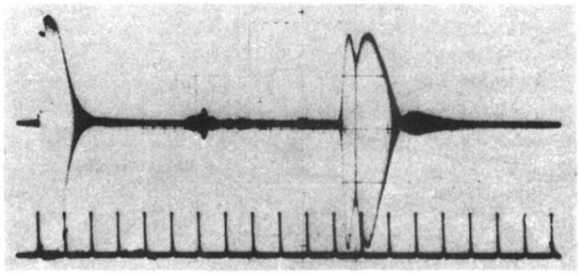

FIG. 4. Photograph of an oscilloscope trace showing a small longitudinal pulse with a time of flight of 55 $\mu$sec and a large transverse pulse with a time of flight of 113 $\mu$sec.

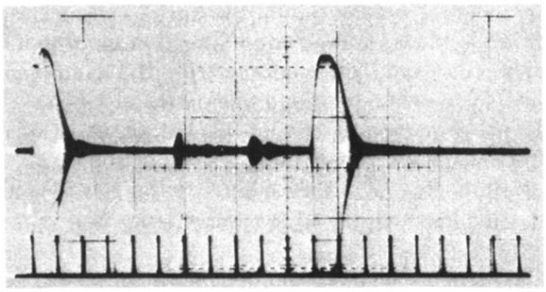

FIG. 5. Photograph of an oscilloscope trace showing a longitudinal pulse at 56 $\mu$sec, a small transverse pulse at 85 $\mu$sec, and a large transverse pulse at 110 $\mu$sec.